Inner-shell photoionization of alkaline-earth-metal atoms

M. Kutzner, D. Winn, and S. Mattingly
Department of Physics, Andrews University, Berrien Springs, Michigan 49104
(Received 25 September 1992; revised manuscript received 8 February 1993)

The photoionization cross sections, branching ratios, and angular-distribution asymmetry parameters for the inner shells of alkaline-earth-metal atoms have been calculated using the relativistic random-phase approximation and the relativistic random-phase approximation modified to include relaxation effects. Our main purpose is to determine whether relaxation effects are important throughout the group IIA of alkaline-earth metals. Comparisons are made between relaxed and unrelaxed results. Results for beryllium and strontium are compared with experiments. Strong relaxation effects are noted for the ionization of $3d$ electrons in barium.

PACS number(s): 32.80.Hd

I. INTRODUCTION

Interest in photoionization from inner shells of atoms and ions has grown rapidly in recent years, due largely to the growing availability of synchrotron-radiation sources [1]. While currently there is a significant amount of photoionization data in the x-ray region of the spectrum [2], there is a limited amount of data near the inner-shell thresholds of most atoms. Yet it is in the vicinity of photoionization thresholds where many of the interesting correlation effects (e.g., exchange, interchannel coupling, relaxation, and polarization) occur [3].

The discovery of interesting correlation effects near the inner-shell thresholds of xenon, barium, and some of the lanthanides has motivated much study [4]. The $4d$ subshells of xenon and barium are both characterized by a broad, delayed absorption peak approximately 50-eV wide above the $4d$ ionization threshold, often referred to as a giant shape resonance [4]. Photoelectron spectroscopy measurements of xenon [5] and barium [6] in this region indicate that a significant fraction of the absorption is due to satellites and multielectron ionization. Theoretical studies employing many-body perturbation theory (MBPT) [7,8] and the relativistic random-phase approximation modified to include relaxation effects (RRPAR) [9,10] have demonstrated that reasonable agreement with experiment can be obtained when relaxation effects are accounted for in these cases.

In addition to the photoionization cross sections, the photoelectron angular-distribution asymmetry parameters β are also important. Although seemingly less affected by relaxation effects than the cross sections [9], they are strongly affected by interchannel coupling, providing an important additional check on the accuracy of the correlated matrix elements. The effects of higher multipoles are also more apparent in the angular-distribution asymmetry parameter than in the cross section, where interference terms in the matrix elements do not appear [11].

In this paper, we investigate the photoionization cross sections and angular-distribution asymmetry parameters for some of the inner shells of alkaline-earth-metal atoms. The focus is on the penultimate shells; however, for Sr and Ba we have analyzed the photoionization of the $3d$ electrons. Specifically, we note the effects of relaxation on these cross sections and β parameters. Section II is a discussion of the methods used in the calculations. In Sec. III we present the photoionization results and in Sec. IV we discuss some of the implications of the study.

II. METHODS

The relativistic random-phase approximation (RRPA) have proven useful for the study of many closed-shell systems, especially the noble gases [12]. Configuration interaction (CI) in the ground states and ionic final states of alkaline-earth-metal atoms complicates the photoionization spectrum in the energy regions just above the valence thresholds. Analysis of alkaline-earth-metal atomic spectra in these regions requires the use of theories which include CI either explicitly or implicitly, e.g., the multiconfiguration relativistic random-phase-approximation theory (MCRRPA) [13], the close-coupling technique [14,15], the configuration-interaction method [16], the multiconfiguration Tamm-Dankoff (MCTD) approximation [17], the hyperspherical-coordinate approach [18], MBPT [19], or multichannel quantum-defect theory (MQDT) [20,21]. Such effects are expected to play a relatively less important role at higher energies, for example, above the ionization threshold of the first inner shell. Hence, for inner-shell photoionization of alkaline-earth-metal atoms, it is anticipated that the RRPA should provide a reasonably good description.

In the RRPA, the partial photoionization cross section for a given subshell is given by

$$\sigma_{n\kappa}=\frac{4\pi^2\alpha\omega}{3}(|D_{nj\rightarrow j-1}|^2+|D_{nj\rightarrow j}|^2+|D_{nj\rightarrow j+1}|^2)\ . \quad (1)$$

Here n is the principal quantum number, $\kappa=\mp(j+\frac{1}{2})$ for $j=l\pm\frac{1}{2}$, where j and l are the single-electron total and orbital angular-momentum quantum numbers. The dipole matrix element $D_{nj\rightarrow j'}$ is the reduced RRPA dipole matrix element for the photoionization channel $nj\rightarrow j'$.

The angular-distribution asymmetry parameter $\beta_{n\kappa}$ for

the subshell $n\kappa$ is defined in terms of the differential cross section

$$\frac{d\sigma_{n\kappa}}{d\Omega}=\frac{\sigma_{n\kappa}(\omega)}{4\pi}[1-\tfrac{1}{2}\beta_{n\kappa}(\omega)P_2(\cos\theta)]\ , \tag{2}$$

where ω is the photon energy and θ is the angle measured between the directions of the incident photon and the photoelectron. A detailed account of the RRPA has been given elsewhere [22].

The importance of allowing for relaxation of the core electrons in photoionization of some systems has been demonstrated previously [23]. As a photoelectron is leaving the atom, the electrons remaining in the ionic core relax from neutral-atom orbitals to orbitals appropriate for the ion. Near the photoionization threshold where the photoelectron speeds are low, it is reasonable to assume that the relaxation process is complete. This effect may be approximated by calculating the continuum photoelectron orbitals in the potential of the relaxed ion. Such calculations have been carried out for xenon [7] and barium [24] in low-order MBPT, in the generalized random-phase approximation with exchange (GRPAE) modified to include relaxation effects [3], and in the relativistic random-phase approximation modified to include these effects (RRPAR) [9,10]. The fully relaxed calculations are not expected to be a good description of photoionization at energies far above threshold since the photoelectrons will have left the vicinity of the ion before relaxation occurs. In this case frozen-core calculations are more realistic.

When the subshell from which the electron is removed has two possible j values (e.g., $p_{1/2},p_{3/2}$ or $d_{3/2},d_{5/2}$), it becomes somewhat arbitrary as to which subshell should contain the hole of the relaxed ion. However, since the shell with $j=l+\frac{1}{2}$ has a lower ionization energy and also represents the most populated of the two subshells, we have chosen to place the hole in the subshell with largest j. The results depend only very weakly on which subshell is chosen.

Also in calculations with relaxed orbitals, overlap integrals $\prod_i\langle\phi_i'|\phi_i\rangle^{q_i}$ between orbitals of the ground state ϕ_i and the corresponding orbitals of the final state ϕ_i' need to be included in the RRPAR matrix element for each subshell i of the ion with occupation number q_i. Inclusion of these overlap integrals is important in determining partial photoionization cross sections and has been accounted for in these calculations. Note that we have not included overlap integrals between orbitals of the ground state and the continuum orbital of the final state. Hence the effects of Auger processes have not been removed from the partial cross sections [25].

Strict RRPA calculations make use of the absolute values of the Dirac-Hartree-Fock (DHF) eigenvalues for the photoionization thresholds. Calculations including relaxation effects, however, were performed using the difference in the total relativistic self-consistent energies of the neutral atom and the ion (so-called $\Delta E_{\rm SCF}$ energies) for the photoionization thresholds. The DHF and $\Delta E_{\rm SCF}$ energies used here were obtained using the Oxford multiconfiguration Dirac-Fock code of Grant *et al.* [26].

TABLE I. Photoionization thresholds in a.u. for subshells of alkaline-earth-metal atoms included in the present calculations.

			Threshold		
Atom	Shell	J	DHF[a]	$\Delta E_{\rm SCF}$[b]	Expt.[c]
Be	1*s*	1/2	4.733	4.533	4.542
	2*s*	1/2	0.3093		0.3426
Mg	2*s*	1/2	3.780		3.55
	2*p*	1/2	2.288	2.080	2.126
	2*p*	3/2	2.277	2.069	2.116
	3*s*	1/2	0.2534		0.2810
Ca	3*s*	1/2	2.262		
	3*p*	1/2	1.349	1.250	1.274
	3*p*	3/2	1.334	1.236	1.261
	4*s*	1/2	0.1963		0.2246
Sr	3*p*	1/2	11.08		10.59
	3*p*	3/2	10.67		10.23
	3*d*	3/2	5.622	5.256	5.292
	3*d*	5/2	5.558	5.189	5.229
	4*s*	1/2	1.949		
	4*p*	1/2	1.126	1.049	1.072
	4*p*	3/2	1.080	1.004	1.037
Ba	3*d*	3/2	30.30	29.60	
	3*d*	5/2	29.71	29.03	
	4*s*	1/2	10.26		
	4*p*	1/2	8.099		
	4*p*	3/2	7.513		
	4*d*	3/2	3.914		3.712
	4*d*	5/2	3.813		3.62

[a]Absolute value of single-particle eigenvalue from Dirac-Hartree-Fock (DHF) calculations.
[b]Difference of self-consistent DHF calculations for ground state and ionic state.
[c]Reference [27].

Table I contains DHF, $\Delta E_{\rm SCF}$, and the experimental threshold energies obtained using photoelectron spectroscopy [27] for all the channels incorporated in the present calculations.

III. RESULTS

A. Beryllium

There have been previous calculations of the photoionization of atomic beryllium from both the valence shell [28] and the inner 1*s* shell [29]. Recently, Krause and Caldwell [30] have partitioned the *K*-shell photoionization cross section of beryllium using photoelectron spectroscopic techniques. They have found that although most of the oscillator strength is due to the mainline channel $[1s^22s^2(^1S)\rightarrow 1s2s^2(^2S)kp(^1P)]$ resulting in the ground-state ion, photoionization-with-excitation channels can contribute as much as 30% near the satellite thresholds at a photon energy of approximately 4.74 a.u. Double-electron resonances have also been shown to be an important component of the beryllium cross section [29]; the effect of these bound-excited states has not been included in the present calculation and so we expect the

agreement of RRPA and RRPAR with experiment to be limited.

Channels included in this calculation were

$$1s_{1/2} \rightarrow \epsilon p_{3/2}, \epsilon p_{1/2} ,$$

$$2s_{1/2} \rightarrow \epsilon p_{3/2}, \epsilon p_{1/2} .$$

Since all transitions from all subshells have been included in the calculation and coupled together the length and velocity results are identical for the RRPA. In the RRPAR, this equality is no longer assured. For beryllium, we find that length and velocity agree to within 3.5%. Since length and velocity are in good agreement, only a single curve representing the geometric mean is shown from each of our calculations.

Our intent here is to demonstrate the effect of relaxation on the K-shell photoionization. The $1s_{1/2}$ partial photoionization cross-section calculations of the RRPA and RRPAR are shown in Fig. 1 along with the experimental measurements of Krause and Caldwell [30]. The experimental results, which were not absolute, have been scaled to the RRPA calculation at 140 eV (5.145 a.u.). In Ref. [29] the experiment was scaled to Hartree-Fock calculations at 140 eV. It is apparent from these calculations that relaxation effects are not very important in K-shell photoionization except for a threshold shift. It is much more important to take photoionization-with-excitation channels into account explicitly to obtain good agreement with experiment near threshold.

The overlap integrals used in the calculations including relaxation are significant. In this case they amounted to approximately a 22% reduction in the $1s_{1/2}$ partial cross section. The $2s$ cross section is not large in this region, amounting to only 6% of the $1s$ cross section near threshold and only 4.5% at 5.5 a.u. We do not show the angular-distribution asymmetry parameter for $1s$ photoionization since it does not deviate significantly from the value 2.0.

B. Magnesium

Calculations for the inner shells of magnesium have been carried out before in the RRPA [20,31]. Unfortunately, as is frequently the case, experimental data for inner-shell photoionization is not available for comparison. The ground state for neutral Mg is $1s^2 2s^2 2p^6 3s^2$. Photoionization channels included in the present magnesium calculations were

$$2s_{1/2} \rightarrow \epsilon p_{3/2}, \epsilon p_{1/2} ,$$

$$2p_{1/2} \rightarrow \epsilon d_{3/2}, \epsilon s_{1/2} ,$$

$$2p_{3/2} \rightarrow \epsilon d_{5/2}, \epsilon d_{3/2}, \epsilon s_{1/2} ,$$

$$3s_{1/2} \rightarrow \epsilon p_{3/2}, \epsilon p_{1/2} .$$

The total photoionization cross-section calculations for Mg are shown in Fig. 2(a). The result for the total RRPA cross section is in agreement with an earlier calculation by Deshmukh and Manson [20], and the partial cross section for $2p_{1/2}$ (not shown) agrees with a more recent calculation by Nasreen, Manson, and Deshmukh [31]. The threshold used for the relaxed calculation is the ΔE_{SCF} energy and is thus lower than the DHF eigenvalue used for the RRPA threshold. Calculations were not carried out in the spectral region just below the $2s$ threshold because of the existence of autoionizing resonances in that region. The effect of relaxation is to lower the cross section near threshold and displace oscillator strength to higher photoelectron energies. Although the results look similar above the DHF threshold at 2.3 a.u., if these two cross sections were plotted as a function of photoelectron energy, the relaxed result would be much lower than the unrelaxed result in the near-threshold region. The region between the two thresholds contains autoionization resonances and has been omitted from the calculations.

The RRPAR total cross section and partial cross sections for the $2p_{3/2}$, $2p_{1/2}$, and $3s_{1/2}$ plus $2s_{1/2}$ subshells

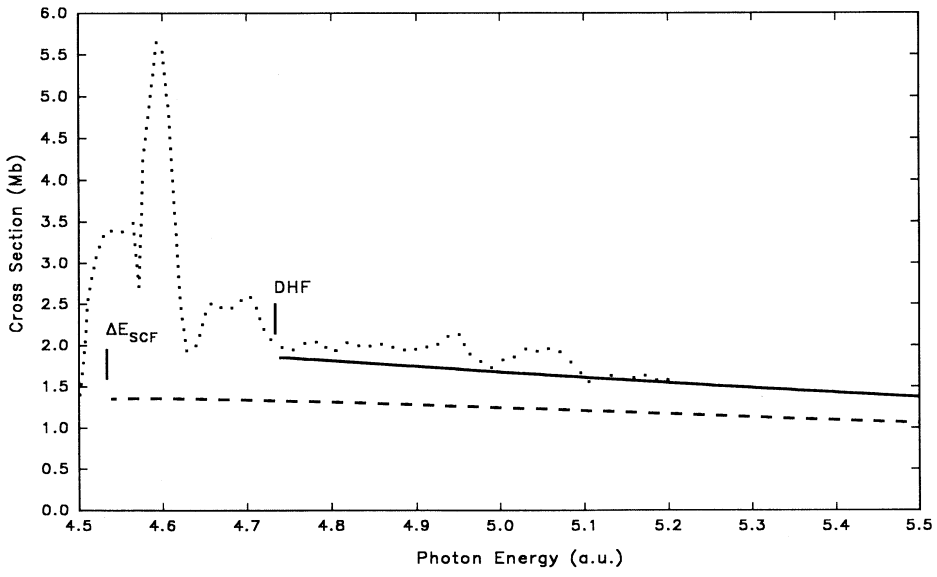

FIG. 1. Partial photoionization cross sections for K-shell ionization of beryllium. RRPA is represented by a solid line. RRPAR is represented by a dashed line. Geometric mean of length and velocity has been taken. Experiment by Krause and Caldwell [30] is represented by a dotted line and has been scaled to the RRPA at 140 eV (5.145 a.u.). DHF and ΔE_{SCF} are the thresholds used for the RRPA and RRPAR calculations respectively.

are plotted in Fig. 2(b). The total cross section is the sum of all singly excited channels listed above with the reduction due to overlap integrals excluded. In this way the oscillator strength due to doubly excited channels is included approximately in the total. Examination of the branching ratios $\gamma=\sigma(2p_{3/2})/\sigma(2p_{1/2})$ in Fig. 2(c) shows that the relaxed results differ slightly from the statistical ratio of 2 near threshold and that both relaxed and unrelaxed branching ratios approach 2 for higher photon energies. Relaxed and nonrelaxed angular-distribution asymmetry parameters β_{2p} are very similar to each other [see Fig. 2(d)] except for the shift in threshold. Here β_{2p} is obtained from $\beta_{2p3/2}$ and $\beta_{2p1/2}$ by taking the weighted average

$$\beta_{2p}=\frac{\sigma_{2p_{3/2}}(\omega)\beta_{2p_{3/2}}(\omega)+\sigma_{2p_{1/2}}(\omega)\beta_{2p_{1/2}}(\omega)}{\sigma_{2p_{3/2}}(\omega)+\sigma_{2p_{1/2}}(\omega)} . \quad (3)$$

It has been suggested that photoionization cross sections of inner shells remain virtually unaffected by the removal of outer-shell electrons, i.e., electrons with a higher principal quantum number, except for a shift of threshold corresponding to a change in outer screening [31]. The argument is that $\langle r \rangle$ for a given subshell (where most of the probability distribution of the subshell is concentrated) depends most strongly on principal quantum number n and very little else. Thus the inner-shell electron orbitals are unchanged by the removal of outer-shell electrons. While this seems to hold for the total photoionization cross section, it may not necessarily hold for the partial cross sections of inner-shell ionization when relaxation effects are considered. Upon photoionizing an inner-shell electron, it is the outermost shell of electrons which undergoes the greatest rearrangement, because of a small effective nuclear charge Z_{eff}. The potential for the outgoing photoelectron is thus changed more when the complete outer shell is present than when it is absent or partially absent as in the case of positive ions. The emergence of substantial overlap integrals for calculations including relaxation greatly reduce the cross section in some instances [8]. The reduction due to overlap integrals is often due primarily to changes in the valence

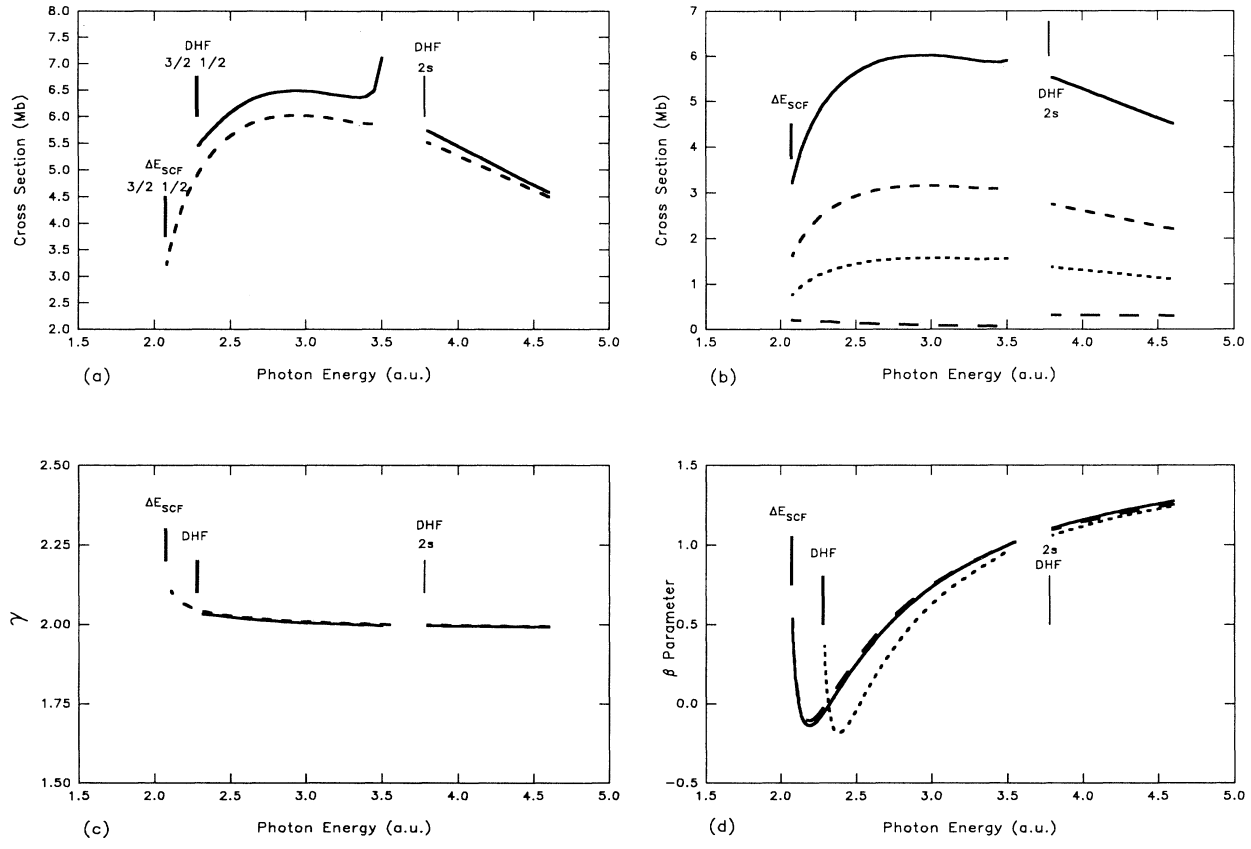

FIG. 2. Photoionization parameters above the $2p$ ionization threshold of atomic magnesium. (a) Total photoionization cross sections in the RRPA (solid line) and RRPAR (dashed line). (b) Total photoionization (solid line), $2p_{3/2}$ partial cross section (short-dashed line), $2p_{1/2}$ partial cross section (dotted line), and $2s+3s$ partial cross sections (long-dashed line) in the RRPAR. (c) $2p_{3/2}$:$2p_{1/2}$ branching ratios γ for Mg $2p$ calculated in the RRPA (solid line) and RRPAR (dashed line). (d) Photoelectron angular-distribution asymmetry parameters β calculated in the RRPA length (dotted line) formulation and in the RRPAR length (solid line) and velocity (dashed line) formulations. Geometric means of length and velocity results were used for cross sections and branching ratios. Thresholds used for RRPA are indicated as DHF and thresholds used for RRPAR are indicated as ΔE_{SCF}.

orbital where Z_{eff} is small; thus one would not expect that the overlap integrals resulting from a calculation of, say, $2p$ photoionization of Mg ($1s^2 2s^2 2p^6 3s^2$) would be similar to those resulting from $2p$ photoionization of Mg^{2+} ($1s^2 2s^2 2p^6$) where the $\langle 3s' | 3s \rangle$ overlap integral does not contribute. The overlap integrals used in the RRPAR calculation of Mg lead to a reduction in the cross section of approximately 20%. Even for energies well above threshold, where relaxation effects are unimportant, photoionization-with-excitation channels which depend strongly on the presence of the valence electrons will remove oscillator strength from the mainline channels. Thus, although the total photoionization cross section may not depend strongly on the presence of the outer shell of s electrons, the partial cross sections do.

C. Calcium

RRPA calculations of photoionization cross sections, angular-distribution asymmetry parameter $\beta_{n\kappa}$, and spin-polarization parameters for the penultimate subshell of neutral calcium were previously reported by Deshmukh and Johnson [21]. The ground-state configuration is [Ar] $4s^2$. Channels included in the present RRPA and RRPAR calculations were

$$3s_{1/2} \rightarrow \epsilon p_{3/2}, \epsilon p_{1/2} ,$$

$$3p_{1/2} \rightarrow \epsilon d_{3/2}, \epsilon s_{1/2} ,$$

$$3p_{3/2} \rightarrow \epsilon d_{5/2}, \epsilon d_{3/2}, \epsilon s_{1/2} ,$$

$$4s_{1/2} \rightarrow \epsilon p_{3/2}, \epsilon p_{1/2} .$$

The total cross sections calculated in the RRPA and RRPAR are plotted together in Fig. 3(a). The effect of relaxation on the $3p$ subshell is to reduce the slope of the cross section near threshold, but not in a dramatic fashion. Absorption oscillator strength is again displaced to higher energies. The partial cross sections computed in the RRPAR and shown in Fig. 3(b) specify how much of the absorption is distributed to the various channels.

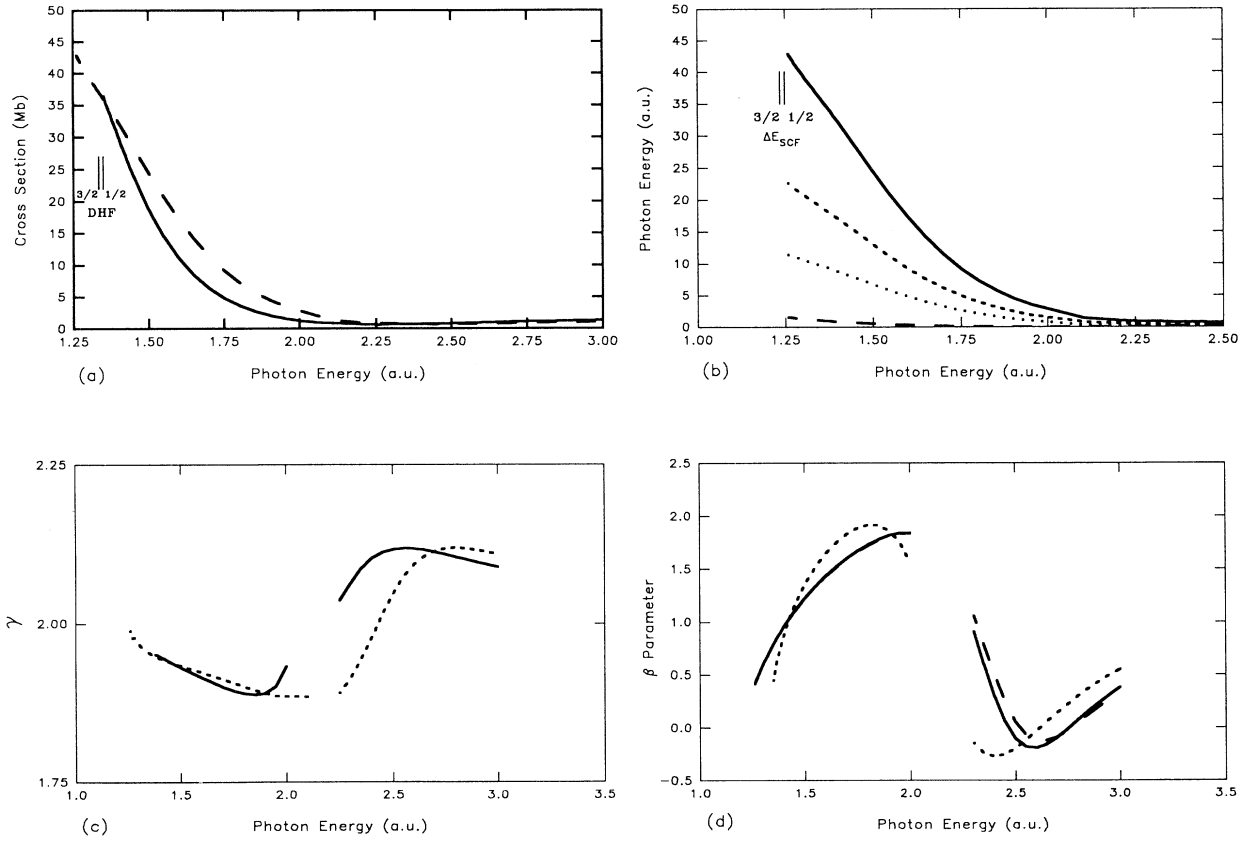

FIG. 3. Photoionization parameters above the $3p$ thresholds for calcium. (a) Total photoionization cross sections in the RRPA (solid line) and RRPAR (dashed line). (b) Total photoionization cross section (solid line), $3p_{3/2}$ partial cross section (short-dashed line), $3p_{1/2}$ partial cross section (dotted line), and $4s$ partial cross section (long-dashed line) in the RRPAR. (c) $3p_{3/2}$:$3p_{1/2}$ branching ratio γ in the RRPA (solid line) and RRPAR (dashed line). The gap between 2.0 and 2.25 a.u. is the region of autoionizing resonances leading up to the $2s$ threshold. (d) Photoelectron angular-distribution asymmetry parameters β. The dotted line represents the RRPA length calculation (length and velocity are virtually indistinguishable); the solid and dashed lines represent the RRPAR length and velocity results respectively. Geometric means of length and velocity have been taken for cross sections and branching ratios. DHF and ΔE_{SCF} indicate the thresholds for the RRPA and RRPAR, respectively.

At threshold, the mainline channels for $3p$ photoabsorption account for approximately 79% of the total absorption. The $4s$ channel represents a mere 4%. The remaining 17% is the reduction due to the overlap integrals and is a rough approximation to the absorption due to photoionization-with-excitation and double-photoionization channels.

The RRPA and RRPAR branching ratios, $\gamma = \sigma(3p_{3/2})/\sigma(3p_{1/2})$, are shown in Fig. 3(c). In the nonrelativistic approximation this ratio is given by the statistical ratio of the occupation numbers of the two subshells, i.e., the constant value 2. Deviations from the statistical value are due almost entirely to the split in threshold energies between the $3p_{3/2}$ and $3p_{1/2}$ channels. Initially $\gamma < 2$ because the $3p_{3/2}$ channel begins at a lower energy than the $3p_{1/2}$ channel. The variations from the statistical ratio become more pronounced near the Cooper minima of the two channels. The Cooper minimum in the $3p_{3/2}$ cross section causes the numerator of γ to become small first. The Cooper minimum in the $3p_{1/2}$ channel then causes the denominator of γ to become small. For the relaxed result, these variations occur at higher energy because of the displacement of oscillator strength to higher energies.

The angular distribution asymmetry parameters β_{3p} as calculated in both the RRPA and RRPAR are plotted in Fig. 3(d). Length and velocity agreement in the RRPA is nearly perfect so only the length result is shown. For the RRPAR calculation, both length and velocity are plotted. It is interesting to note that interference between the $3p \rightarrow \epsilon d$ channels and the $3p \rightarrow \epsilon s$ channels causes the β parameter in calcium to behave quite differently from the β_{2p} of magnesium, where β drops suddenly just above threshold. Also note that the effect of relaxation on β is to cause it to rise less rapidly from the threshold than the unrelaxed result.

D. Strontium

Whereas photoionization of the valence electrons of strontium has been the subject of numerous studies over the years, little theoretical work has been done on inner-shell photoionization for this system. Experimental photoabsorption studies near the $3d$ threshold were performed by Mansfield and Connerade [32], who found that the spectrum is dominated by the presence of a strong

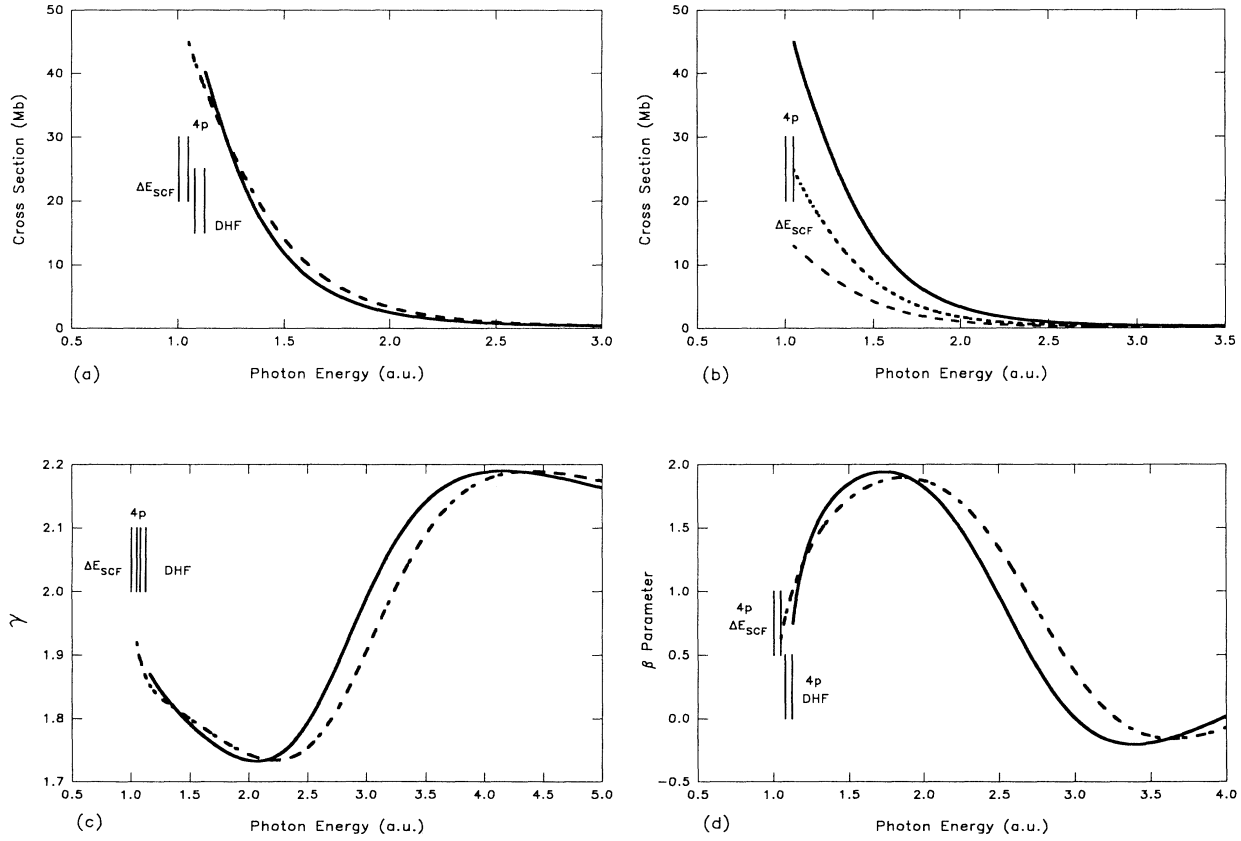

FIG. 4. Photoionization parameters above the $4p$ thresholds of Sr. (a) Total photoionization cross sections in the RRPA (solid line) and RRPAR (dashed line). (b) Total photoionization cross section (solid line), $4p_{3/2}$ partial cross section (dotted line), and $4p_{1/2}$ partial cross section (dashed line) in the RRPAR. (c) $4p_{3/2}$:$4p_{1/2}$ branching ratios γ in both the RRPA (solid line) and RRPAR (dashed line). (d) Photoelectron angular-distribution asymmetry parameters β in the RRPA (solid line) and the RRPAR (dashed line).

$3d$-ϵf shape resonance. Recently, Koizumi *et al.* [33] have obtained photoion yield spectra of Sr which appear similar to the previous photoabsorption results except at higher energies, where they diverge.

The ground state for Sr is [Kr] $5s^2$. Eighteen jj-coupled channels were included in the present truncated RRPA and RRPAR calculations. They are

$$3p_{1/2} \rightarrow \epsilon d_{3/2}, \epsilon s_{1/2} ,$$

$$3p_{3/2} \rightarrow \epsilon d_{5/2}, \epsilon d_{3/2}, \epsilon s_{1/2} ,$$

$$3d_{3/2} \rightarrow \epsilon f_{5/2}, \epsilon p_{3/2}, \epsilon p_{1/2} ,$$

$$3d_{5/2} \rightarrow \epsilon f_{7/2}, \epsilon f_{5/2}, \epsilon p_{3/2} ,$$

$$4s_{1/2} \rightarrow \epsilon p_{3/2}, \epsilon p_{1/2} ,$$

$$4p_{1/2} \rightarrow \epsilon d_{3/2}, \epsilon s_{1/2} ,$$

$$4p_{3/2} \rightarrow \epsilon d_{5/2}, \epsilon d_{3/2}, \epsilon s_{1/2} .$$

Total photoionization cross sections above the $4p$ thresholds are shown in Fig. 4(a). The resemblance between the Sr $4p$ cross sections and the Ca $3p$ cross sections (Fig. 3) is striking. The effects of relaxation are similar in both cases also. Photoionization of the $2p$ electrons in Mg (see Fig. 2), however, differs greatly from the Ca $3p$ and Sr $4p$ cross sections. This may be because the $2p$ wave functions in the ground state of Mg have no nodes whereas the $3p$ and $4p$ wave functions in the ground states of Ca and Sr have one node and two nodes, respectively.

The partial cross sections, branching ratios γ, and β parameters for $4p$ photoionization of Sr shown in Figs. 4(b)–4(d) are also very similar to the corresponding results for $3p$ of Ca. Apparently, screening by electrons interior to $4p$ in Sr yields a similar Z_{eff} to that experienced by $3p$ electrons in Ca. The overlap integrals in this instance reduce the partial cross sections by approximately 15%.

The relaxed and unrelaxed total photoionization cross sections for Sr above the $3d$ thresholds are presented in Fig. 5(a) along with the photoabsorption measurements

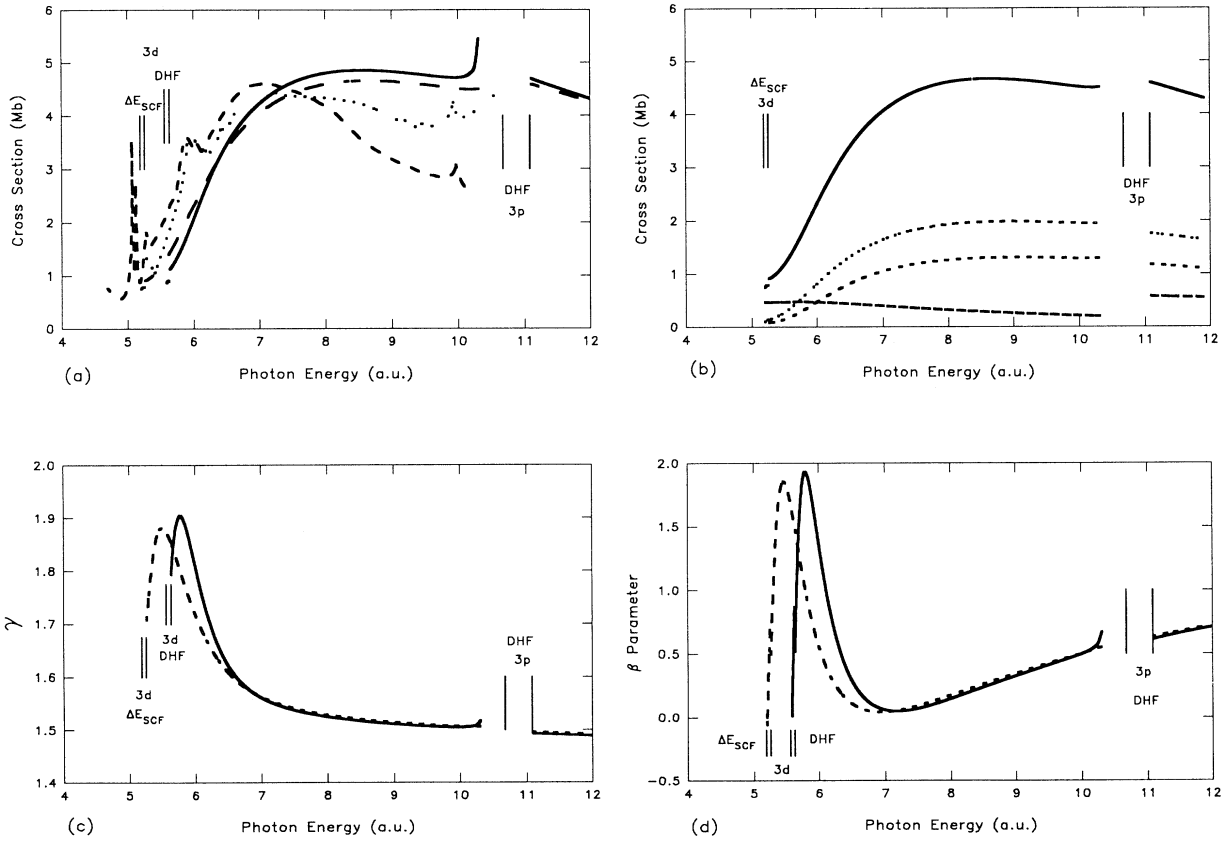

FIG. 5. Photoionization parameters above the $3d$ thresholds of Sr. (a) RRPA calculations are represented by the solid line; RRPAR calculations are represented by the long-dashed line; photoabsorption measurements [32] are represented by the short-dashed line; photoion yield measurements [33] are represented by the dotted line. (b) Total photoionization cross section (solid line), $3d_{5/2}$ partial cross section (dotted line), $3d_{3/2}$ partial cross section (short-dashed line) and sum of all other single-excitation cross sections (long-dashed line) in the RRPAR. (c) $3d_{5/2}$:$3d_{3/2}$ branching ratios γ in both the RRPA (solid line) and the RRPAR (dashed line). (d) Photoelectron angular-distribution asymmetry parameters β. The solid line represents the RRPA calculation; the dashed line represents the RRPAR result.

of Mansfield and Connerade [32] and the photoion yield spectrum of Koizumi *et al.* [33]. The experimental results have been scaled to match each other and the RRPAR calculation at approximately 200 eV. It might be expected that relaxation effects would play an important role for $3d$ photoionization of Sr because of the large $3d$-ϵf shape resonance. Comparison of the RRPA and RRPAR results, however, does not show this to be the case. The RRPA and RRPAR are reasonably consistent with one another.

There are a few notable differences between the theoretical results and the experiments. The autoionization resonances and double-electron resonances seen in the experimental results are not reproduced by the theory, although a portion of the first resonance below the $3p$ threshold can be seen in the RRPA result. The theory also does not predict the amount of downturn in the cross section measured by both the photoabsorption experiment and the photoion yield experiment. The theories seem to compare most favorably with the photoabsorption experiment [32].

Partial cross sections for $3d$ photoionization are shown in Fig. 5(b). It is interesting that near the $3d$ threshold, centrifugal barrier effects in the photoelectron potential cause the $3d$ partial cross sections to be very small compared with the combined cross sections of $4s$ and $4p$. The overlap factor here is approximately 23%, indicating that double-excitation processes are important.

The $3d_{5/2}$:$3d_{3/2}$ branching ratios γ shown in Fig. 5(c) deviate quite significantly from the statistical value of 3:2 near threshold. They are also quite different from the branching ratios for $4p$ photoionization. This is because, unlike the $4p$ cross section which decreases immediately above threshold, the $3d$ cross sections are increasing above threshold. Since the $3d_{5/2}$ cross section begins rising approximately 0.065 a.u. before the $3d_{3/2}$ cross section due to spin-orbit splitting, the branching ratio begins above the statistical value of 3:2. However, eventually the $3d_{5/2}$ partial cross section reaches its peak and begins to get smaller and the branching ratio drops below 3:2. The peak in the branching ratio is slightly more broadened in the RRPAR result because of the more delayed onset of photoabsorption in the relaxed model.

The photoelectron angular distribution asymmetry parameter β for the $3d$ subshell of Sr is shown in Fig. 5(d). It is fairly typical of β parameters from d subshells [7–10]. Aside from a shift in threshold, the energy dependence of β is not much different in the RRPAR than in the RRPA.

E. Barium

Photoionization of the $4d$ inner subshell of barium has been a showcase for various many-body theories. The importance of relaxation and polarization in this case has been well established [3,8,10,23]. The present calculations are for $3d$ photoionization and demonstrate that relaxation effects are very important for this subshell as well. Unfortunately, the wealth of experimental data which exists above the $4d$ threshold is not available above the $3d$ threshold; it is hoped that these calculations and the availability of new synchrotron sources will motivate further studies of the deeper inner subshells of Ba and other systems in the near future.

The $3d$ subshells are tightly bound with DHF thresholds of 29.71 and 30.30 a.u. for the $3d_{5/2}$ and $3d_{3/2}$ subshells, respectively. Thus x-rays are required for photoionization from these deep inner shells. One might anticipate that photoionization from deep inner shells would be simplified relative to photoionization from less tightly bound shells. For xenon, however, it was found that the effects of relaxation were just as important (perhaps more important) for the $3d$ subshells as it was for the $4d$ subshells [9,34]. Here we find a similar result for Ba.

The 19 coupled channels included in the Ba calculations were

$$3d_{3/2} \rightarrow \epsilon f_{5/2}, \epsilon p_{3/2}, \epsilon p_{1/2} ,$$

$$3d_{5/2} \rightarrow \epsilon f_{7/2}, \epsilon f_{5/2}, \epsilon p_{3/2} ,$$

$$4s_{1/2} \rightarrow \epsilon p_{3/2}, \epsilon p_{1/2} ,$$

$$4p_{1/2} \rightarrow \epsilon d_{3/2} , \epsilon s_{1/2} ,$$

$$4p_{3/2} \rightarrow \epsilon d_{5/2}, \epsilon d_{3/2}, \epsilon s_{1/2} ,$$

$$4d_{3/2} \rightarrow \epsilon f_{5/2}, \epsilon p_{3/2}, \epsilon p_{1/2} ,$$

$$4d_{5/2} \rightarrow \epsilon f_{7/2}, \epsilon f_{5/2}, \epsilon p_{3/2} .$$

The $3p_{3/2}$ and $3p_{1/2}$ channels were excluded since the photoionization thresholds are at 40.167 and 42.956 a.u., respectively, far from the region under consideration; interchannel coupling between $3p$ and $3d$ channels is therefore expected to be minimal near the $3d$ thresholds.

The total RRPA and RRPAR cross sections in the vicinity of the $3d$ thresholds are shown in Fig. 6(a). Here the spin-orbit splitting is large enough that there is a region between the $3d_{5/2}$ and $3d_{3/2}$ thresholds that is free of resonances and we have included cross section calculations in this region. It is clearly seen in Fig. 6(a) that relaxation has shifted the oscillator strength toward higher energies. The unrelaxed RRPA calculation is very large just above the $3d_{5/2}$ threshold and very small with a positive slope just above the $3d_{3/2}$ threshold. For the relaxed RRPAR calculation, the cross section is quite different. Above the $3d_{5/2}$ threshold, the cross section is much smaller than in the RRPA; above the $3d_{3/2}$ threshold, however, there is a significant increase in the cross section relative to the RRPA result.

The component partial cross sections in the RRPAR are shown in Fig. 6(b). As expected, the largest partial cross section is the $3d_{5/2}$ followed by $3d_{3/2}$. However, the other singly excited channels especially $4d$ channels are nearly as important throughout the region. It is also expected that doubly excited channels are importance since the overlap integrals reduce the partial cross sections by 25%. This value is similar to the one found for $4d$ photoionization of Ba [9].

Branching ratios for $3d_{5/2}$:$3d_{3/2}$ are shown in Fig. 6(c). The spin-orbit splitting is large in this case (0.6 a.u.). Hence, at energies just above the $3d_{3/2}$ threshold, the

$3d_{5/2}$ partial cross section has become somewhat level. The branching ratio thus assumes the character of the $3d_{3/2}$ partial cross section.

Photoelectron angular-distribution asymmetry parameters β are shown in Fig. 6(d) for both the RRPA and RRPAR calculations. In the region between the $3d_{5/2}$ and $3d_{3/2}$ thresholds, β is plotted for just $3d_{5/2}$. Above the $3d_{3/2}$ threshold, we utilized the weighted average for β as prescribed in Eq. (3). The main differences between the RRPA and RRPAR occur just above the thresholds. Inspection shows that the model with the largest cross section just above a threshold has a corresponding β parameter which takes a steeper downward turn.

IV. DISCUSSION

There are a number of interesting points to be noted from this study of inner-shell photoionization of alkaline-earth-metal atoms. First, it is interesting to note that the total photoionization cross sections calculated in the RRPA and RRPAR converge at higher energies for each species of alkaline-earth-metal atom. This shows that the details of the potential experienced by the photoelectron become less important when the photoelectron is removed rapidly. This merging of the RRPA and RRPAR total cross sections seems to be delayed when the difference between the DHF and ΔE_{SCF} energies is large, e.g., the $3d$ subshells of Sr and Ba.

It is also interesting to note the differences between the $2p$ photoionization cross section of Mg and the $3p$ and $4p$ cross sections of Ca and Sr, respectively. The Mg $2p$ cross section begins with positive slope whereas the Ca and Sr cross sections have nearly identical shapes beginning with a negative slope. This may be due to the difference in the number of nodes in the ground-state orbitals.

Most of the cases of photoionization examined in this study have not manifested large relaxation effects. Barium is the exception to this. As in the case of $4d$ photoionization of Ba, the $3d$ photoionization cross section is profoundly affected by relaxation effects. In $4d$ photoionization, it was found that the potential for ϵf electrons has a centripetal barrier delaying the onset of photoemission above the threshold; relaxation effects were found to enhance the centripetal barrier [4]. Presumably, the effect of relaxation on the potential is similar in the case

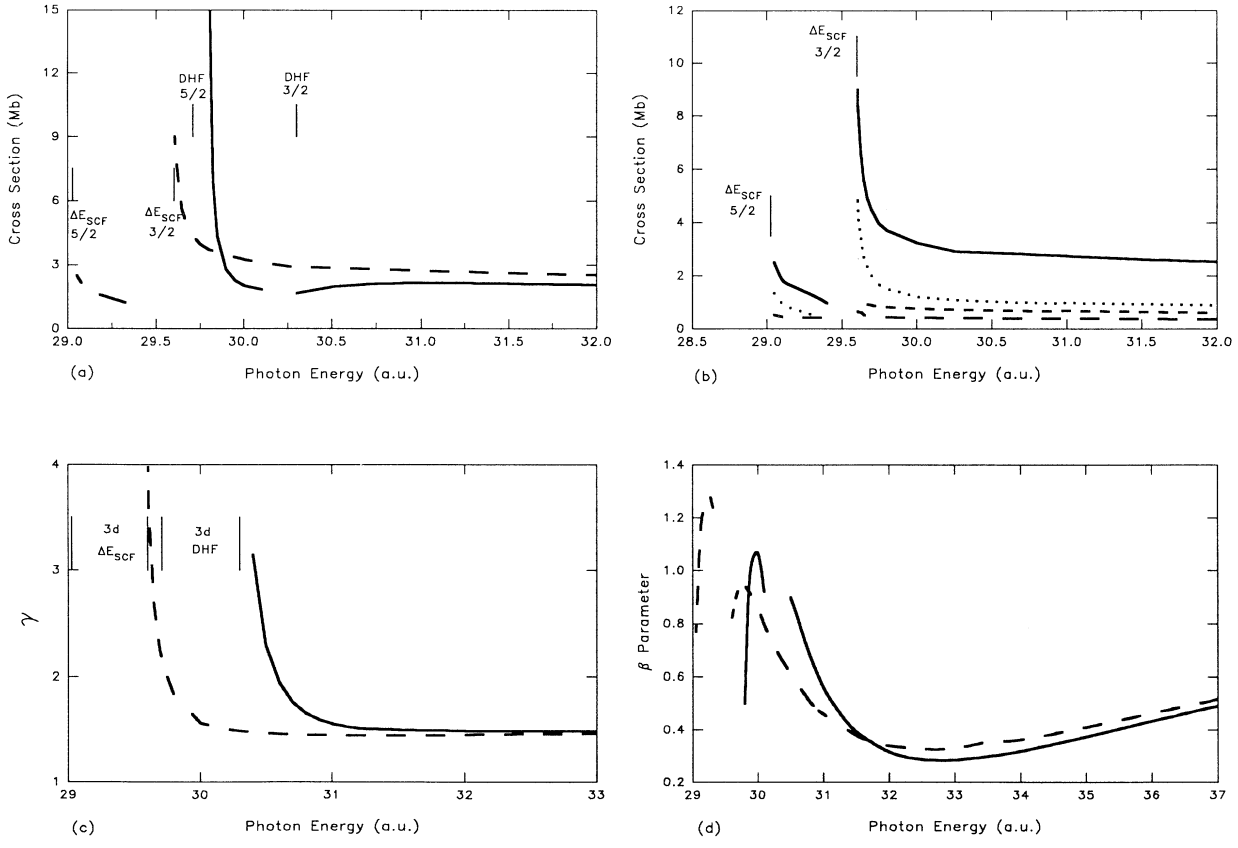

FIG. 6. Photoionization parameters above the $3d$ subshell thresholds of atomic Ba. (a) Total photoionization cross sections in the RRPA (solid line) and the RRPAR (dashed line). Gaps in the calculations below the $3d_{3/2}$ thresholds are regions of autoionizing resonances and were not calculated. (b) Total photoionization cross section (solid line), $3d_{5/2}$ partial cross section (dotted line), $3d_{3/2}$ partial cross section (short-dashed line), and sum of all other single-excitation channels (long-dashed line) in the RRPAR. (c) $3d_{5/2}$:$3d_{3/2}$ branching ratios γ in both the RRPA (solid line) and the RRPAR (dashed line). (d) Photoelectron angular-distribution asymmetry parameters β in the RRPA (solid line) and RRPAR (dashed line).

of $3d$ photoionization, although more study is needed to establish this. Analysis of these cases is important in order to predict which other systems are likely to show large relaxation effects.

Although experimental results are not available for most of the cases studied here, there are results for $3d$ photoionization of Sr [32,33]. The agreement between experiment and theory in this case is only fair. Near threshold, both the RRPA and RRPAR are in reasonable agreement with experiment; however, at higher energies the theories are well above the experiments. It is not clear whether this is due to some aspect of the experiments or if an important effect is missing from the theories.

ACKNOWLEDGMENTS

We wish to thank the late Hugh P. Kelly for his important contributions to this field of study. We also thank Vojaslav Radojevic for his development of the RRPAR method and Walter Johnson for the use of the RRPA computer code. This work was supported by NSF Grant No. PHY-9014012.

[1] See, for example, *X-Ray and Inner-Shell Processes,* edited by T. A. Carlson, M. O. Krause, and S. T. Manson, AIP Conf. Proc. No. 215 (AIP, New York, 1991).

[2] E. B. Saloman, J. H. Hubbell, and J. H. Scofield, At. Data Nucl. Data Tables **38**, 1 (1987).

[3] M. Ya. Amusia, *Atomic Photoeffect,* translated by K. T. Taylor (Plenum, New York, 1990).

[4] See, for example, *Giant Resonances in Atoms, Molecules and Solids,* Vol. 151 of *NATO Advanced Study Institute, Series B: Physics,* edited by J. P. Connerade, J. M. Esteva, and R. C. Karnatak (Plenum, New York, 1987).

[5] U. Becker, D. Szostak, H. G. Kerkhoff, M. Kupsch, B. Langer, R. Wehlitz, A. Yagishita, and T. Hayaishi, Phys. Rev. A **39**, 3902 (1989); D. W. Lindle, T. A. Ferret, P. A. Heimann, and D. A. Shirley, *ibid.* **37**, 3808 (1988); U. Becker, T. Prescher, E. Schmidt, B. Sonntag, and H. E. Wetzel, *ibid.* **33**, 3891 (1986).

[6] J. M. Bizau, D. Cubaynes, P. Gerard, and F. J. Wuilleumier, Phys. Rev. A **40**, 3002 (1989); M. Richter, M. Meyer, M. Pahler, T. Prescher, E. V. Raven, B. Sonntag, and H. E. Wetzel, *ibid.* **39**, 5666 (1989); U. Becker, in *Giant Resonances in Atoms, Molecules, and Solids,* Vol. 151 of *NATO Advanced Study Institute, Series B: Physics,* edited by J. P. Connerade, J. M. Esteva, and R. C. Karnatak (Plenum, New York, 1987), p. 473.

[7] Z. Altun, M. Kutzner, and H. P. Kelly, Phys. Rev. A **37**, 4671 (1988).

[8] M. Kutzner, Z. Altun, and H. P. Kelly, Phys. Rev. A **41**, 3612 (1990).

[9] M. Kutzner, V. Radojević, and H. P. Kelly, Phys. Rev. A **40**, 5052 (1989).

[10] V. Radojević, M. Kutzner, and H. P. Kelly, Phys. Rev. A **40**, 727 (1989).

[11] S. T. Manson, Argonne National Laboratory Report No. ANL/APS/TM-8, 1990, p. 38 (unpublished).

[12] W. R. Johnson and K. T. Cheng, Phys. Rev. A **20**, 978 (1979).

[13] K.-N. Huang and W. R. Johnson, Phys. Rev. A **25**, 634 (1982); W. R. Johnson and K. N. Huang, Phys. Rev. Lett. **48**, 315 (1982).

[14] D. L. Moores, Proc. Phys. Soc. London **91**, 830 (1967); **88**, 843 (1966).

[15] P. Scott, A. E. Kingston, and A. Hibbert, J. Phys. B **16**, 1983.

[16] P. L. Altick, Phys. Rev. **169**, 21 (1968).

[17] V. Radojević and W. R. Johnson, Phys. Rev. A **31**, 2991 (1985).

[18] C. H. Greene, Phys. Rev. A **23**, 661 (1981).

[19] H. P. Kelly, Phys. Rev. B **136**, 896 (1964); Z. Altun, S. L. Carter, and H. P. Kelly, Phys. Rev. A **27**, 1943 (1983); D. Frye and H. P. Kelly, J. Phys. B **20**, L677, (1987); Z. Altun, Phys. Rev. A **40**, 4968 (1989).

[20] P. C. Deshmukh and S. T. Manson, Phys. Rev. A **28**, 209 (1983).

[21] P. C. Deshmukh and W. R. Johnson, Phys. Rev. A **27**, 326 (1983).

[22] W. R. Johnson and C. D. Lin, Phys. Rev. A **20**, 964 (1979).

[23] G. Wendin, Phys. Lett. **51A**, 291 (1975); M. Ya. Amusia, V. K. Ivanov, and L. V. Chernysheva, Phys. Lett. **59A**, 191 (1976).

[24] H. P. Kelly, S. L. Carter, and B. E. Norum, Phys. Rev. A **25**, 2052 (1982).

[25] T. Åberg and G. Howat, in *Corpuscles and Radiation in Matter I,* edited by W. Mehlhorn, Handbuch der Physik Vol. 31 (Springer-Verlag, Berlin, 1982), p. 469.

[26] I. P. Grant, B. J. McKenzie, P. H. Norrington, D. F. Mayers, and N. C. Pyper, Comput. Phys. Commun. **21**, 207 (1980).

[27] H. Siegbahn and L. Karlsson, in *Corpuscles and Radiation in Matter I,* edited by W. Mehlhorn, Handbuch der Physik Vol. 31 (Springer-Verlag, Berlin, 1982), p. 215.

[28] H.-C. Chi and K.-N. Huang, Phys. Rev. A **43**, 4742 (1991).

[29] H. P. Saha and C. D. Caldwell, Phys. Rev. A **40**, 7020 (1989); F. Bely-Dubau, J. Dubau, and D. Petrini, J. Phys. B **10**, 1613 (1977).

[30] M. O. Krause and C. D. Caldwell, Phys. Rev. Lett. **59**, 2736 (1987).

[31] G. Nasreen, S. T. Manson, and P. C. Deshmukh, Phys. Rev. A **40**, 6091 (1989).

[32] M. W. D. Mansfield and J. P. Connerade, Proc. R. Soc. London Ser. A **342**, 421 (1975).

[33] T. Koizumi, T. Hayaishi, Y. Itikawa, Y. Itoh, T. Matsuo, T. Nagata, Y. Sato, E. Shigemasa, A. Yagishita, and M. Yoshino, J. Phys. B **23**, 403 (1990).

[34] M. Ya Amusia, in *Advances in Atomic and Molecular Physics,* edited by D. Bates and B. Bederson (Academic, New York, 1981), Vol. 170, p. 2.